PCCP

ROYAL SOCIETY OF CHEMISTRY

PAPER

View Article Online
View Journal | View Issue

Cite this: *Phys. Chem. Chem. Phys.*, 2022, **24**, 10069

Influence of vanillic acid immobilization in Nafion membranes on intramembrane diffusion and structural properties†

Blake Trusty,[a] Samuel Berens,[a] Ahmad Yahya,[b] Junchuan Fang,[b] Sarah Barber,[b] Anastasios P. Angelopoulos,*[b] Jonathan D. Nickels*[b] and Sergey Vasenkov*[a]

Received 7th March 2022,
Accepted 29th March 2022

DOI: 10.1039/d2cp01125e

rsc.li/pccp

Pulsed field gradient (PFG) NMR in combination with quasielastic neutron scattering (QENS) was used to investigate self-diffusion of water and acetone in Nafion membranes with and without immobilized vanillic acid (VA). Complementary characterization of these membranes was performed by small angle X-ray scattering (SAXS) and NMR relaxometry. This study was motivated by the recent data showing that an organic acid, such as VA, in Nafion can preserve its catalytic activity in the presence of water even at high intra-polymer water concentrations corresponding up to 100% ambient relative humidity. However, there is currently no clear understanding of how immobilized organic acid molecules influence the microscopic transport properties and related structural properties of Nafion. Microscopic diffusion data measured by PFG NMR and QENS are compared for Nafion with and without VA. For displacements smaller than the micrometer-sized domains previously reported for Nafion, the VA addition was not observed to lead to any significant changes in the water and/or acetone self-diffusivity measured by each technique inside Nafion. However, the reported PFG NMR data present evidence of a different influence of acetone concentration in the membranes with and without VA on the water permeance of the interfaces between neighboring micrometer-sized domains. The reported diffusion data are correlated with the results of SAXS structural characterization and NMR relaxation data for water and acetone.

1. Introduction

Nafion is a commercially available perfluorosulfonic acid (PSA) polymer, which is well known due to its potential and/or current applications as an ion exchange membrane,[1–4] solid super acid catalyst[5,6] and chemical (acetone) sensor for breath analysis,[7–10] among others. The structure of Nafion membranes consists of a continuous hydrophobic semi-crystalline matrix and interfacial perfluoroalkyl ether (PFE) regions with sulfonic groups.[11–17] The later groups participate in the formation of hydrophilic channels allowing for fast diffusion of water (*viz.* water channels). At sufficiently large intramembrane water concentrations these water channels can form an interconnected network allowing for an unhindered water transport through an entire membrane. Recent experimental data show that while water diffuses through these channels, less polar molecules can diffuse through an interfacial region formed by the PFE side chains between the hydrophobic semi-crystalline matrix and hydrophilic water channels.[4,18,19]

The use of Nafion in heterogeneous catalysis has typically been restricted to organic solvents such as acetone due to deprotonation and consequent deactivation of the perfluorosulfonic acid groups in water.[20–22] It was recently demonstrated that an immobilization of an organic acid, such as vanillic acid (VA), in Nafion can preserve its catalytic activity in the presence of water even at high intra-polymer water concentrations corresponding up to 100% ambient relative humidity.[10] This discovery has enabled significant advances in the use of Nafion as an optode to monitor the dynamic evolution of biomarkers of metabolic health such as acetone in the humid environment of exhaled human breath.[23] However, there is currently no clear understanding of how immobilized organic acid molecules influence the microscopic transport and related structural properties of Nafion. To close this gap, we used pulsed field gradient (PFG) NMR in combination with quasielastic neutron scattering (QENS) to investigate diffusion of water and acetone on different microscopic length scales in Nafion. Complementary characterization of Nafion membranes was performed by small angle X-ray scattering (SAXS) and NMR relaxometry for water and

[a] *Department of Chemical Engineering, University of Florida, Gainesville, FL 32611, USA. E-mail: svasenkov@che.ufl.edu; Tel: +1 352 392 0315*
[b] *Department of Chemical and Environmental Engineering, University of Cincinnati, Cincinnati, OH 45221, USA*

† Electronic supplementary information (ESI) available. See DOI: https://doi.org/10.1039/d2cp01125e

acetone molecules. The results of our studies indicate that in VA-functionalized Nafion membranes, the immobilized VA molecules as well as acetone molecules are preferentially located in the interfacial PFE regions between water channels and the crystalline matrix of Nafion. Our PFG NMR diffusion data show evidence of a different influence of acetone concentration in the membranes with and without VA on the water permeance of the interfaces between neighboring micrometer-sized domains, which were previously reported for non-functionalized Nafion.[19] The diffusion and structural data for the latter membranes, which were the focus of our recent paper,[19] are compared with those presented in the current work for VA-functionalized Nafion membranes. Clearer understanding of the fundamental transport mechanisms of acetone and water in Nafion is expected to play a prominent role in the expanded use of Nafion as a polymeric membrane catalyst.

2. Experimental methods

2.1 Preparation of samples of Nafion membranes

Nafion 117 (Fuel Cell Store) was prepared in the following way. Nafion membrane was cut into desired size and submerged into 5% hydrogen peroxide solution. The membranes remained submerged in this solution for 1 hour at 90 °C and then rinsed repeatedly in deionized water to remove any impurities. The membranes were subsequently immersed in 0.5 M sulfuric acid solution for 1 hour at 90 °C to ensure full protonation of the membrane. Functionalization of these membranes with VA was done as follows. Saturated VA solution was prepared by adding 300 mg VA into 100 mL deionized water. The previously prepared Nafion membranes were cut into proper size for NMR measurements, around 120 mg with a length of approximately 4 cm. To immobilize VA into the membrane, the cut membranes were placed into a Petri dish containing 20 mL of the saturated VA solution, and permitted to soak for 31 minutes at room temperature, then quickly rinsed with deionized water to remove excess surface acid.

To determine the amount of vanillic acid imbibed into the membrane, extraction in ethanol was employed. The procedure was as follows: the VA-loaded membranes were dried overnight before attainment of a UV-Vis spectrum *via* an Ocean Optics HR2000+CG-UV-NIR Spectrometer, employing an Ocean Optics DH-2000-BAL light source. Membranes were subsequently submerged for approximately 2 days in 5 mL of 200 proof ethanol. The resultant solution was attenuated into range for spectroscopic resolution *via* dilution and analyzed, as were the post-extraction membranes after they were dried overnight. An ethanol stock solution was prepared by weighing ~0.022 g of vanillic acid into a 100 mL flask and diluting to the mark with ethanol. This stock solution was subsequently further diluted with ethanol to obtain a calibration solution set of varying, known vanillic concentration. A calibration was also carried out for the saturated aqueous vanillic acid solution to confirm that the calculated concentration of vanillic acid was within experimental error of reported literature values.[24] A partition coefficient of 1.9 was obtained for the membrane relative to that in the saturated solution. The corresponding VA intra-membrane concentration was found to be $(1.3 \pm 0.1) \times 10^{-2}$ mmol g^{-1}.

Samples for NMR studies were prepared by placing approximately 120 mg of Nafion 117 membrane pieces into a thin-wall 5 mm NMR tube (Wilmad-LabGlass). The NMR tube was attached to a custom vacuum manifold for 4 h to degas and partially remove water from the membranes at 60 mTorr and 298 K. After degassing and partial water removal, desired amounts of acetone (Sigma-Aldrich, HPLC grade) and deionized water were added to the membrane through condensation of acetone and water vapor from the calibrated volume of the vacuum system using liquid N_2. After loading, the samples were flame-sealed and allowed to equilibrate for over 24 h at 298 K before any measurements were performed.

A similar membrane activation procedure was also used to prepare membrane samples for SAXS and QENS studies. Membrane samples were dried under vacuum for around 4 h at 298 K prior to addition of acetone and/or D_2O. Loading was performed in an inert (He) glovebox with the membranes placed in an aluminum envelope and placed in an annular sample can with defined sample space of 1 mm and closed using an indium seal. Control samples, acetone-free Nafion membranes with and without VA and D_2O were measured, in addition to the experimental samples with acetone. These samples were used to represent the elastic scattering component of the spectra, but also serve to provide a check against residual water influence within the Nafion materials. Residual water would be equally present in the background controls and experimental samples, so its contribution would be removed. However, as will be shown later in the paper, the controls did not show any strong Q-dependence in the scattering, indicating that there was not a substantial signal from any residual water content. Based on NMR measurements, the residual water content was estimated to be around 0.7 mmol g^{-1}. For SAXS and QENS studies, a calibrated amount of acetone and/or D_2O were directly added to the membrane samples to reach desired intramembrane concentrations.

2.2 NMR measurements

The majority of ^{1}H NMR measurements were performed on a 17.6 T/750 MHz Avance III HD (Bruker BioSpin wide-bore spectrometer). ^{1}H pulsed field gradient (PFG) NMR measurements on this instrument employed the Diff50 diffusion probe with a GREAT60 gradient amplifier to generate magnetic field gradients up to 20 T m^{-1}. Complimentary ^{1}H PFG NMR measurements were performed on a 14 T/600 MHz AVANCE III HD narrow-bore spectrometer with a Diff30 diffusion probe used to generate magnetic field gradients up to 12 T m^{-1}. Within uncertainty, it was confirmed that the diffusion data measured with the same samples and under identical conditions on both instruments were the same. This agreement is indicative that there are no measurement artifacts under our experimental conditions.

Water and acetone concentrations in Nafion were estimated using a well-known correlation between the area under the

NMR spectrum and the number of the corresponding molecules in a sample. This approach was confirmed to be valid for concentration measurements in non-functionalized Nafion for both water and acetone used in our previous studies.[19] In particular, our data for intramembrane water concentration based on the area under the NMR line were found to match,[19] within uncertainty, to another method of estimating water concentration in Nafion *via* NMR chemical shift measurements.[25] The area under the line approach was successful to estimate intramembrane concentrations of both water and acetone in VA functionalized Nafion based on the following observations: (i) there is no overlap between the water and acetone lines in the recorded NMR spectra, and (ii) our PFG NMR diffusion studies confirmed that there was no liquid water or acetone outside of the membranes in our NMR samples, *i.e.* essentially the entire measured signal corresponded to intramembrane species. The proportionality coefficient between the area under the water and acetone NMR lines and the corresponding concentrations was determined based on the measurements of the NMR spectra of the samples with the known amounts of these molecules, like in our previous studies.[19]

Diffusion measurements employed the 13-interval PFG NMR pulse sequence with bipolar gradients and longitudinal eddy current delays.[26,27] This sequence was chosen as it can reduce or eliminate disturbing effects related to magnetic susceptibility. Sinusoidal shaped gradient pulses with the effective duration of each pulse (δ) between 0.5 and 1.0 ms and gradient amplitudes (g) between 0.3 and 20 T m^{-1} were used. Effective diffusion times (t) ranged from 10 ms to 4 s for both water and acetone diffusion. The value of t was calculated as ($\Delta - \tau/2 - \delta/6$), where Δ and τ denote, respectively, the time intervals between two gradient pulses of equal polarity and between two gradient pulses of opposite polarity in a bipolar pair. Longitudinal eddy current delays of $\sim$6 ms were used to insure the lack of residual magnetic field inhomogeneity during the signal acquisition.

Self-diffusion data were obtained through measurement of PFG NMR attenuation curves. These measure dependences of the PFG NMR signal on the strength of the applied magnetic field gradient, with all other pulse sequence parameters held constant. For cases of normal diffusion with one self-diffusivity (D), PFG NMR signal attenuation can be presented as[26,28]

$$\Psi = \exp(-q^2 tD) \quad (1)$$

where the parameter $q = 4g\gamma_{\text{nucleus}}\delta$ and γ_{nucleus} is the gyromagnetic ratio for a particular nucleus. To calculate values of mean square displacement (MSD), the Einstein relation for three-dimensional diffusion was applied[28]

$$\langle r^2 \rangle = 6Dt \quad (2)$$

The ^{1}H NMR spectra of water and acetone in Nafion 117 membranes each consisted of one line. The observed chemical shift for water was between 7.6 and 9.0 ppm, and for acetone it was at around 1.5 ppm.

Longitudinal (T_1) NMR relaxation times were measured using the standard inversion recovery pulse sequence. Transverse (T_2) NMR relaxation times were measured using the Carr–Purcell–Meiboom–Gill (CPMG) pulse sequence. In all measured samples, the relaxation data for water and acetone showed no distribution over relaxation times for either measured component. The representative NMR relaxation data are shown in Table S1 (ESI†). It is important to note that the T_2 NMR relaxation times in the VA-functionalized samples were by up to around an order of magnitude smaller than those reported in the corresponding non-functionalized Nafion samples (Table S1, ESI†). This resulted in a much lower signal-to-noise ratios of the PFG NMR attenuation data measured for the VA-functionalized samples in comparison to the non-functionalized Nafion samples.[19] All NMR measurements reported in this work were performed at 296 K.

2.3 SAXS measurements

SAXS measurements were performed at the Advanced Photon Source in Argonne National Laboratory, beamline 12-ID-C. Nafion membranes were measured in sealed quartz capillaries with an incident X-ray energy of 18 keV, a sample to detector distance of 2.255 m, and an exposure time of 0.5 s. Data were reduced using Igor Pro to provide one dimensional intensity *versus* scattering wave vector, $\boldsymbol{Q}$. Analysis of SAXS data was performed using the OriginPro suite. The fitting terms consisted of a low-Q power law to account for long length scale structure beyond the range of this measurement, a constant term to represent background scattering, and three Gaussian functions to account for structural correlations – the crystalline phase peak, the ionomer peak and the shoulder of the ionomer peak seen at high Q.

2.4 QENS measurements

QENS measurements were performed at the Spallation Neutron Source in Oak Ridge National Laboratory, using the BASIS instrument.[29] Data were collected in a 'frame-skipping' mode which extends the dynamic range of the instrument by rejecting every other pulse from the neutron source. The membrane was first sealed into an aluminum envelope and then placed within a 0.5 mm gap between an inner spacer and the sample can. The measurements were performed at 296 K for non-functionalized and VA-functionalized Nafion membranes with different quantities of acetone and D_2O added. Data was reduced using Mantid[30] using a vanadium standard, and empty can scattering was subtracted. The resulting data reported scattered intensity as a function of scattering wave vector, $\boldsymbol{Q}$, and energy transfer, ω. Data were analyzed using DAVE[31] with a Lorentzian function used to represent broadening due to molecular diffusion of acetone. From the observed linewidths, the full width at half max (FWHM) of the Lorentzian function can be converted to the time domain *via* Plank's constant, $\hbar$. The diffusion coefficient can be obtained then as a function of scattering wave vector, $\boldsymbol{Q}$, *via* the relation $D(\boldsymbol{Q}) = \text{FWHM}(q)/(2\hbar q^2)$.

3. Results and discussion

Fig. 1 shows representative examples of ^{1}H PFG NMR attenuation curves for acetone (Fig. 1A) and water (Fig. 1B) in the VA-

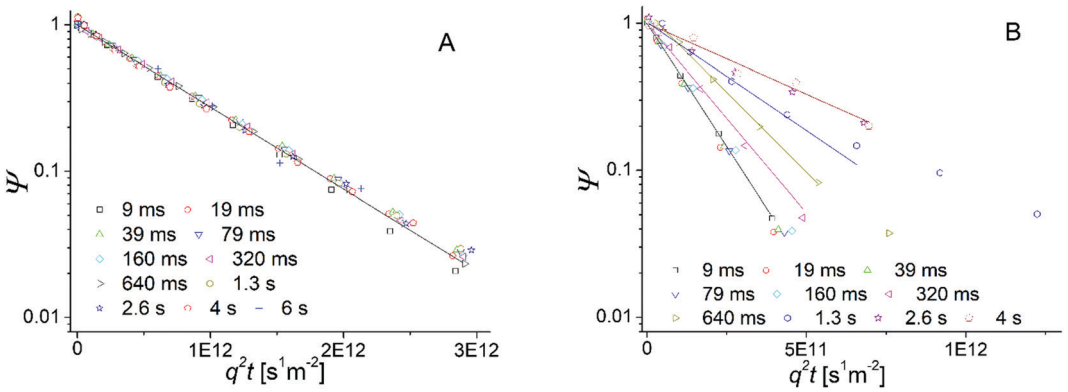

Fig. 1 Examples of ^{1}H PFG NMR attenuation curves for acetone (A) and water (B) in a VA functionalized Nafion membrane at 296 K. The intramembrane concentrations of acetone and water were 0.47 mmol g^{-1} and 1.4 mmol g^{-1}, respectively. Solid lines represent the best fit lines using eqn (1) for the range of the diffusion times showing coinciding data, within uncertainty. Dotted lines are the best fit lines using eqn (1) of the initial parts of the attenuation curves, which show deviations from the monoexponential behavior. These initial parts correspond to an essentially monoexponential behavior, within uncertainty.

functionalized Nafion membranes at 296 K. In Fig. 1A, the monoexponential shape of the attenuation curves, which appear as straight lines in the presentation of the figure, is in agreement with eqn (1). It is seen that the attenuation data for acetone in Fig. 1A coincide across multiple diffusion times used, indicating a self-diffusivity that is independent of diffusion time, within uncertainty. Least squares fitting of these data using eqn (1) for each diffusion time resulted in a separate acetone self-diffusivity for every diffusion time used. These self-diffusivities are plotted as a function of root MSD (RMSD) in Fig. 2. Here and later the values of RMSD were obtained using the Einstein relation (eqn (2)). Fig. 2 shows an independence of the acetone self-diffusivity of the RMSD across the entire RMSD range used.

In contrast with the attenuation data for acetone, the attenuation curves for water demonstrate coincidence for different diffusion times and the monoexponential behavior only in the limit of short ($\leq$160 ms) and long ($\geq$3 s) diffusion times (Fig. 1B). In the intermediate time range, the attenuation curves show deviations from the monoexponential behavior. In this intermediate range the water effective (average) self-diffusivity, which is defined by the initial slope of the attenuation curve,[19,25,26] decreases with increasing diffusion time (Fig. 1B). Such behavior is in a qualitative agreement with our diffusion data observed for water in non-functionalized Nafion loaded with acetone/water mixtures at similar water and acetone concentrations as those used in the current work.[19] As discussed in our previous study of diffusion in non-functionalized Nafion, this behavior can be explained by diffusion of water along water channels, which are not fully interconnected in the entire membrane. In this case, micrometer-sized domains of interconnected water channels are expected to exist. These domains are separated by transport barriers, which represent water channel regions with a reduced water concentration.[19]

Protons, which enter Nafion as parts of water molecules, can diffuse inside Nafion not only as parts of these molecules, but also as parts of other species, including SO_3H^+ and H_3O^+.[32] This happens due to proton exchange processes in Nafion. Such proton exchange processes, however, are expected on a much shorter time scale in comparison to the millisecond time scale used in our PFG NMR measurements.[33,34] As a result, proton exchange processes cannot explain the observed time dependence of the PFG NMR diffusion data.[19]

To quantify the PFG NMR diffusion data for water, an entire attenuation curve (when no deviations from the monoexponential behavior are observed) or only an initial part of the attenuation curve[19,28,35] (when there are deviations from the monoexponential behavior) were fitted to eqn (1) for each diffusion time used. The resulting water self-diffusivities are shown in Fig. 2 as a function of RMSD for different acetone concentrations used in our study and water concentration of around 2 mmol g^{-1}. The same diffusion data were also plotted as a function of diffusion time and presented in Fig. S1 (ESI†).

As discussed above, the self-diffusivity of acetone is independent of RMSD, within uncertainty, in the entire range of

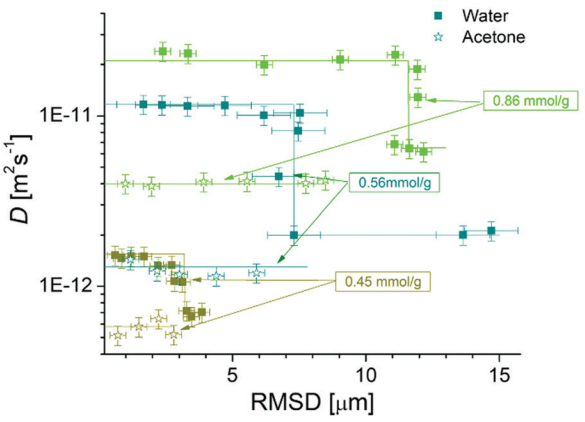

Fig. 2 Dependence of the measured self-diffusivities of acetone (stars) and water (squares) on root MSD in VA-functionalized Nafion membranes at 296 K. Water concentration in Nafion was held constant at ~2 mmol g^{-1}. Solid lines are guidelines shown as visual aids.

RMSDs studied (Fig. 2). In contrast, for water there is no dependence of the self-diffusivity on RMSD at short displacements, then a rapid transition occurs to the much lower values of the self-diffusivities at larger displacements. These data can be used to estimate sizes of the domains of the interconnected water channels and permeance of the domain boundaries, *viz.* transport barriers separating neighboring domain, in the same way as in our previous work focused on non-functionalized Nafion.[19] As discussed in this previous work, the average size (N) of the domains of interconnected water channels can be estimated as the RMSD value corresponding to the transition from the decreasing to constant self-diffusivity, which corresponds to the limiting self-diffusivity at large RMSDs.[19] This estimate is based on conclusions from previously published Monte Carlo (MC) simulations of diffusion in a lattice separated into cubic domains of equal size, in which the boundaries of these domains represent permeable transport barriers.[36] The values of N estimated using this approach are reported in Table 1.

Table 1 shows that at a constant, within uncertainty, water concentration the value of N tends to increase with increasing acetone concentration. Such behavior was observed for two water concentrations around 2.0 and 1.5 mmol g^{-1}. The permeance of the domain boundary (P) was estimated by assuming that the resistance to diffusion water molecules experience in the limit of long diffusion times is the sum of two resistances in series. The first of these is the resistance associated with the permeance of the domain boundary, and the second is associated with diffusion inside the domains of interconnected water channels.[19,28,37]

$$\frac{1}{D_\infty} = \frac{1}{D_0} + \frac{1}{NP} \quad (3)$$

where D_0 and D_∞ are the time independent (no change in D with changing RMSD) self-diffusivities, respectively, in the limit of small and large RMSDs and the corresponding diffusion times. The data for domain boundary permeance obtained *via* eqn (3) are presented in Table 1.

The values of P were also estimated using the PFG NMR tracer exchange approach,[28] in the same way as in our previous study of non-functionalized Nafion.[19] In this approach, deviations from the monoexponential attenuation behavior were described with the existence of two molecular fractions, each with different self-diffusivities (D_1 and D_∞) and different PFG NMR signal fractions (p_1 and $(1 - p_1)$)[28]

$$\Psi = \mathrm{p}_1 \times \exp(-q^2 t D_1) + (1 - p_1) \times \exp(-q^2 t D_\infty) \quad (4)$$

The ensemble with the faster diffusivity D_1 and its PFG NMR signal fraction p_1 is attributed to molecules remaining inside the same domain of interconnected water channels during the diffusion time used in the PFG NMR experiment. The second of these ensembles corresponds to diffusion through more than one domain with the self-diffusivity that can be estimated as D_∞ and the corresponding signal fraction $(1 - p_1)$. Examples of best fit curves using eqn (4) are shown in Fig. S2 (ESI†) for the same attenuation curves as those presented in Fig. 1B (see data for the intermediate range of diffusion times). The corresponding best fit results are shown in Table S2 (ESI†). It is important to note that under our conditions of the PFG NMR experiment, the PFG NMR signal fractions are expected to correspond to the molecular fractions of each ensemble since there is no distribution over T_1 and T_2 relaxation times for water. Thus, the fraction of molecules (γ)[28] that left the original domain by crossing over the domain boundary should be equal to $(1 - p_1)$. The dependence of γ on diffusion time represents a tracer exchange curve, which has the same meaning as those measured in traditional tracer exchange experiments between confining domains and their surroundings.[28,38] Fig. S3 (ESI†) presents the dependencies of $p_1 = (1 - \gamma)$ on diffusion time. The area under each dependency yields the first statistical moment, which is equal to the time constant of molecular exchange (τ_{ex}), *viz.* the mean lifetime of a molecule inside a given domain. This can be related to the domain boundary permeance as[28,38]

$$\tau_{ex} = \int_{t=0}^{\infty} (1 - \gamma) \mathrm{d}t = \frac{R^2}{15 D_0} + \frac{R}{3P} \quad (5)$$

where the domains are assumed to be spherical with the radius R. Eqn (5) results from adding first moment $\frac{R^2}{15D_0}$ associated with the resistance to transport due to intra-domain diffusion, and the corresponding first moment $\frac{R}{3P}$ associated with the domain surface resistance.[28,38] The values for R were estimated as follows. It is well known that the influence of an external surface of confining domains on intra-domain self-diffusion can be presented, in the first approximation, as a function of the surface-to-volume ratio of these domains.[28,38] This function is not sensitive

Table 1 Average size of domains of interconnected water channels, permeance of the domain boundaries, and time constant of molecular exchange for these domains in VA-functionalized Nafion loaded with acetone and water

Acetone conc. (mmol g^{-1})	H_2O conc. (mmol g^{-1})	Temp. (K)	N (μm)	$P \times 10^6$ (m s^{-1}) using eqn (3)	R (μm)	τ_{ex} (s)	$P \times 10^6$ (m s^{-1}) using eqn (5)
0.45 ± 0.05	2.0 ± 0.4	296	3.2 ± 0.8	0.4 ± 0.1	1.6 ± 0.5	1.2 ± 0.2	0.5 ± 0.1
0.57 ± 0.05	1.8 ± 0.4	296	7.3 ± 1.5	0.4 ± 0.1	3.7 ± 0.8	1.5 ± 0.3	0.4 ± 0.1
0.86 ± 0.10	2.0 ± 0.4	296	16 ± 4	0.5 ± 0.2	8 ± 2	1.8 ± 0.4	0.5 ± 0.2
1.17 ± 0.10	2.1 ± 0.4	296	19 ± 5	0.6 ± 0.2	9 ± 3	2.6 ± 0.5	0.5 ± 0.2
0.21 ± 0.03	1.4 ± 0.3	296	2.0 ± 0.5	0.4 ± 0.1	1.0 ± 0.2	0.5 ± 0.1	0.4 ± 0.1
0.29 ± 0.04	1.6 ± 0.4	296	3.5 ± 0.7	0.4 ± 0.1	1.8 ± 0.3	0.8 ± 0.2	0.4 ± 0.1
0.47 ± 0.05	1.4 ± 0.3	296	14 ± 4	0.6 ± 0.2	7 ± 2	1.6 ± 0.3	0.5 ± 0.2

to the domain shape. Such lack of sensitivity to the shape can be rationalized by noting that the probability for any molecule to be at the domain surface is determined only by the surface-to-volume ratio under the conditions of a uniform intra-domain concentration of diffusing molecules. Noting that for spherical domains of radius R and for cubic domains of side length N the value of the surface-to-volume ratio would be exactly the same when $R = N/2$ we estimated the values of R as $N/2$. Using this estimate, the second term ($R/3P$) in the right hand of eqn (5) was consistently larger than the first one ($R^2/15D_0$). This allowed the estimation of domain boundary permeance using eqn (5) where the contribution of the first term in the right hand-part were taken into account, but were not significant. The resulting values for the domain boundary permeance are shown in Table 1. Within uncertainty, the two methods of estimating the values of P using eqn (3) and (5) are in good agreement (Table 1), which confirms the validity of our estimations.

Our previously published work for non-functionalized Nafion membranes observed an increase in domain boundary permeance with increasing acetone concentration.[19] However with the addition of VA functionalization, Table 1 and Fig. 3 highlight that within uncertainty, the values of P remain the same with changing acetone concentration for a similar range of acetone concentrations as that used in our work for non-functionalized Nafion. This observation will be discussed later in the paper.

Fig. 4 illustrates the effect of VA functionalization on the absolute values of intra-domain water self-diffusivity (D_0) and acetone self-diffusivity in the PFE interfacial regions. Holding acetone concentration constant, within uncertainty, and increasing water concentration increases the self-diffusivities of both diffusing components (Fig. 4), which is in agreement with the previous study in non-functionalized Nafion.[19] The data in Fig. 4 show that, within a relatively large experimental uncertainty in water concentration, the addition of VA has little to no effect on the overall self-diffusivities of either component.

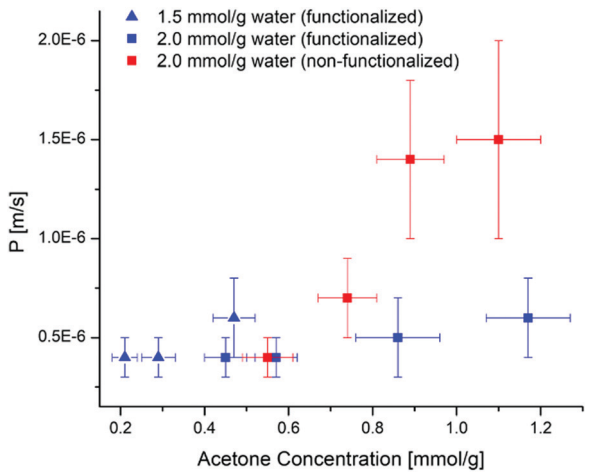

Fig. 3 Estimated values for domain boundary permeance for water with changing acetone concentration at 1.5 mmol g^{-1} water (blue triangles) and 2 mmol g^{-1} water (blue and red squares). Red points indicate values of P estimated for non-functionalized Nafion membranes,[19] while blue points indicate P estimates for Nafion functionalized with VA.

To study an influence of VA addition on the structure of Nafion we have performed complementary SAXS measurements of the VA-functionalized Nafion loaded with acetone and/or water. Fig. 5 shows the average structural correlation from SAXS over 3 water concentrations for the ionomer region where water channels are located (labeled "Ionomer/Water Channel") and for the crystalline backbone region of the Nafion polymer (labeled "Crystalline") as a function of increasing acetone concentration in VA-functionalized Nafion. The corresponding data for non-functionalized Nafion from our previous work[19] are also shown, for comparison.

The data for individual water concentrations over which the average was taken can also be found in Fig. S4 (ESI†). An example fitting of the SAXS spectra is shown in Fig. S5 (ESI†). As discussed in ref. 19, the SAXS correlation length corresponds to a distance between two objects, in this case the cross-sectional dimension of the water channels[39,40] or average spacing between crystalline regions.[41] Hence, the data presented in Fig. 5 suggests that with increasing acetone concentration there is a decrease in the water channel diameter and an increase in the distance between the neighboring crystalline segments due to swelling of the interfacial PFE regions with acetone for both non-functionalized and VA-functionalized Nafion. Indeed, in our previous work the interpretations of the SAXS data under the same loading conditions in non-functionalized Nafion led to the conclusion that acetone occupies the PFE side chain regions of the Nafion polymer, between the crystalline backbone and the hydrophilic water channels. Increasing acetone concentration, therefore, swells these regions, causing the water channels to compress.[19] The data in Fig. 5 also indicate that for the ionomer/water channel region the peak positions for the VA-functionalized Nafion VA tend to be slightly lower or the same, within uncertainty, in comparison to the corresponding data in non-functionalized Nafion. At the same time, for the crystalline region the peak positions for the VA-functionalized Nafion are slightly higher or the same, within uncertainty, in comparison to the corresponding data in non-functionalized Nafion. Hence, we can conclude that the VA functionalization has a similar influence on the peak positions as acetone addition. Consequently, it is likely that VA and acetone occupy the same PFE side chain regions of the Nafion polymer, between the crystalline backbone and hydrophilic water channels. This conclusion is also supported by the observation that upon the addition of VA into Nafion both T_1 and T_2 NMR relaxation times are reduced by a larger factor for acetone than for water under the same conditions (Table S1, ESI†). A schematic presentation of the microscopic Nafion structure, which is supported by these data, is shown in Fig. 6.

Swelling of interfacial PFE regions with acetone (or any other mobile molecules) can increase the diffusion rate of water through interfaces between neighboring domain of interconnected water channels located in these regions. Indeed, we have previously observed and reported an increase in the

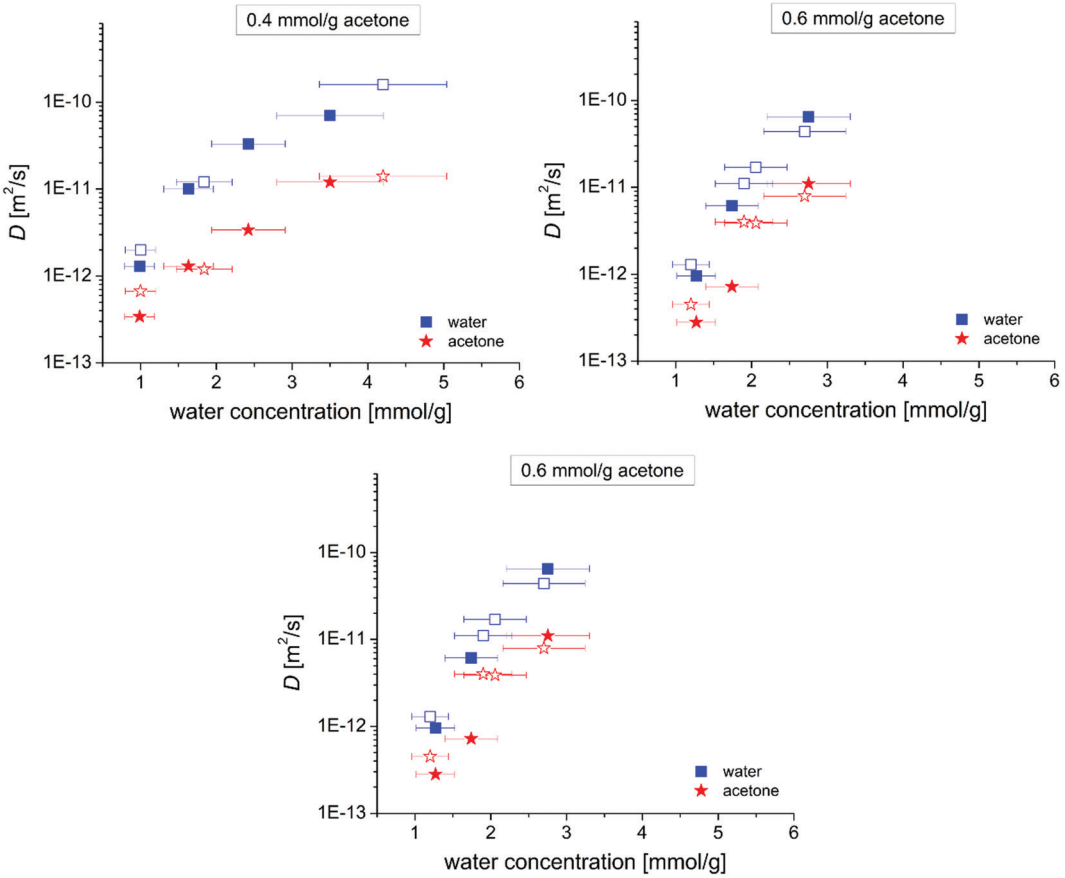

Fig. 4 Self-diffusivities of water in the limit of short diffusion times (blue squares) and acetone (red stars) measured as a function of water concentration in non-functionalized Nafion (filled points) and in VA-functionalized Nafion (empty points). The measurements were performed by PFG NMR at 296 K for three constant, within uncertainty, acetone concentrations shown in the figure. The size of the points indicates uncertainty in the self-diffusion coefficients (D).

permeance of such interfaces with increasing acetone concentration in in non-functionalized Nafion.[19] These data are shown in Fig. 3 to serve as the reference for the corresponding data we report here for VA-functionalized Nafion for the same or similar water and acetone concentrations. The results in Fig. 3 suggest that the VA functionalization negate the effect of acetone on the permeance, *i.e.* an addition of acetone no longer causes an increase in P. This suggests that the diffusion pathways for water and acetone are more separated in the presence of VA, *i.e.* water and acetone molecules do not mix much at the domain boundaries where an increased acetone concentration has a potential of increasing water permeance through the boundaries.

In contrast to the data on the permeance discussed above, the dependence of the intradomain water self-diffusivity (D_0) on acetone concentration at a constant, within uncertainty, water concentration is not influenced significantly by the VA functionalization (Fig. S6, ESI†). It is important to note that the analysis of such dependence is hindered by a large uncertainty of D_0, which is mostly related to the large uncertainty in the water concentration coupled with the existence of a very strong dependence of D_0 on this concentration (Fig. 4). Nevertheless, the data in Fig. S6 (ESI†) are consistent with a somewhat stronger, on average, increase of D_0 values with increasing acetone concentration for the non-functionalized than for the VA-functionalized Nafion. This is in a qualitative agreement with the much stronger for the non-functionalized than for the VA-functionalized Nafion dependence of P on the acetone concentration for the same or similar water concentration (Fig. 3).

Self-diffusion of acetone on the length scales much smaller than those probed by PFG NMR can be directly interrogated by means of QENS. QENS is a spectroscopic technique probing motions occurring from picoseconds (ps) to nanoseconds (ns), over length scales of Angstroms to nanometers by observing the change in momentum of scattered neutrons which gain or lose energy through direct collisions with atomic nuclei in the sample. QENS has previously been used to interrogate the dynamics of water in Nafion materials,[42,43] even examining water motions in a functional fuel cell.[44]

Here, we have measured acetone diffusion in the same Nafion samples as those used in the PFG NMR studies discussed above. Non-functionalized and VA-functionalized Nafion membranes with different acetone and D_2O concentrations were measured at 296 K. The polymer itself was also measured, both with and without VA functionalization. All measurements were performed at 296 K using the backscattering spectrometer

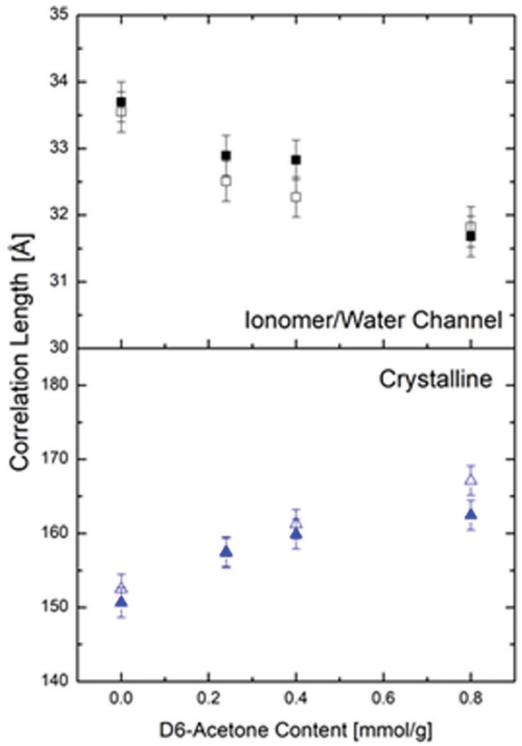

Fig. 5 SAXS correlation lengths averaged over 3 water concentrations (see Fig. S4, ESI†) as a function of acetone concentration in non-functionalized Nafion (filled points) and VA functionalized Nafion (empty points) at 296 K.

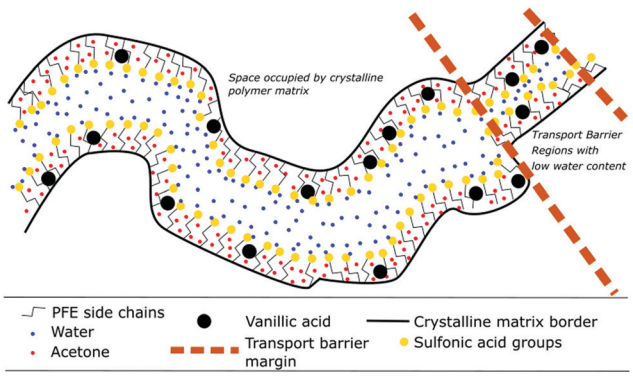

Fig. 6 Schematic presentation of the microscopic structure of Nafion with the preferred locations of water, acetone, and vanillic acid.

(BASIS)[29] at the Spallation Neutron Source (Oak Ridge National Laboratory, Oak Ridge, TN, USA). The predominant signal observed in these experiments was from incoherent scattering of neutrons from the natural isotopic abundance hydrogen in acetone. The incoherent scattering of neutrons is not strong from deuterium, D, or from carbon, oxygen or fluorine atoms; nor would we expect the coherent signal to be a strong contribution.[45]

The resulting QENS spectra are reduced to present the scattered intensity *versus* energy transfer for a series of scattering wave vectors (Fig. S7–S9, ESI†). The data were modeled in the intensity domain using the observations of the base polymer to represent the elastic scattering contribution and a Lorentzian function to represent the quasielastic component. This was performed for each value of the scattering wave vector, $\boldsymbol{Q}$ (from 0.2 $Å^{-1}$ to 2.0 $Å^{-1}$) as seen in Fig. S10 (ESI†). We present the full-width at half-maximum (FWHM) of the Lorentzian distribution used to model the spectra *versus* Q^2. Here, the FWHM can be associated to the average relaxation time of a molecular motion of the acetone and Q is equivalent to an inverse length scale. In Fig. S10 (ESI†), a linear dependence can be seen for these motions. Such behavior indicates that the timescale of the motions of acetone follow a dependence on the length scale squared. The observed motions are thus assumed to be diffusional in nature, though it should be acknowledged that a contribution from reorientational motions may exist, especially at higher values of Q. A difference from prior QENS studies of water dynamics within Nafion materials is the lack of proton localization at the acid groups on the ionomer channel at low solvent volume fractions.[42–44] This strong association of water with the ionomer boundary is seen in a sub-diffusive dynamical mode of the mobile water population which trends to archetypal diffusion (Q^2 dependence of dynamics) at higher water content where both the size of the ionomer channel increases as well as the ratio of water molecules to ionomer groups. The protons in acetone do not participate in ionic associations or hydrogen bonds with the ionomer, this is seen in the discussed above QENS data for acetone which requires only one feature to describe the quasielastic scattering. No strong Q-dependence was observed in the QENS data upon D_2O addition to the Nafion activated samples (Fig. S11, ESI†). The data in Fig. S11 (ESI†) show that any changes from a residual H_2O contribution and/or polymer motion upon D_2O addition are, at most, very small in comparison to the observed acetone dynamics (Fig. S8, ESI†). In all cases the background subtraction was used to remove any influence of such changes on the acetone data.

The QENS data can be converted into a self-diffusion coefficient for each value of Q which is shown in Fig. 7A. This figure demonstrates a roughly constant self-diffusion coefficient for each sample across the displacement length scales probed. We can summarize these data by taking the average value of the self-diffusion coefficient over the entire range of RMSD probed for each sample as shown in Fig. 7B. Three conclusions emerge from this analysis. Firstly, there is an effect of water on short range acetone diffusion probed by QENS. In a qualitative agreement with the PFG NMR data, the QENS results show a tendency for the acetone self-diffusivity to be larger for a larger water concentration. Secondly, there is the decrease in the self-diffusion coefficient for acetone in the membrane samples in comparison to the self-diffusion coefficient of acetone as a bulk liquid. Both with and without D_2O added, acetone is seen to have a self-diffusion coefficient in Nafion that is more than an order of magnitude lower than that in the bulk liquid. Finally, we see that the observed diffusion coefficients for acetone are more than an order of magnitude larger than those measured by PFG NMR for the same or similar total water and acetone concentrations (Fig. 4). This result was observed for both

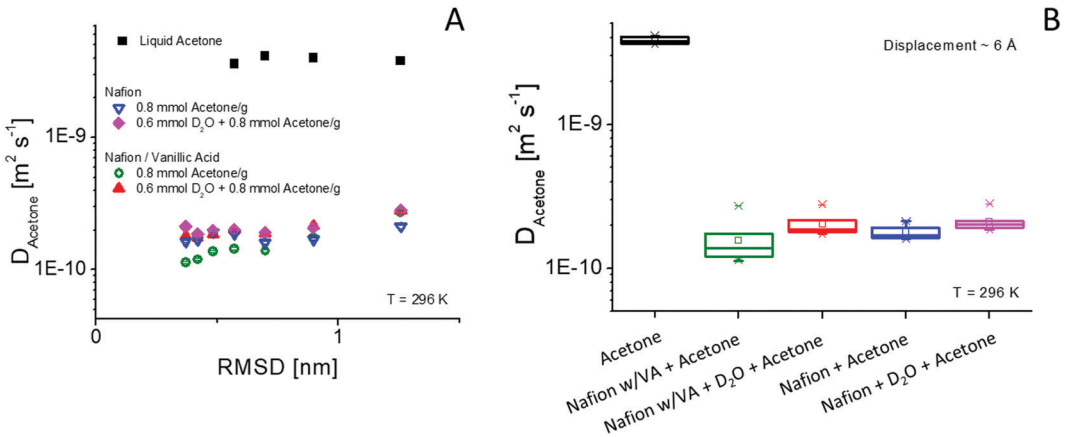

Fig. 7 Acetone self-diffusion coefficients from QENS measurements presented as a function of RMSD (A), and acetone self-diffusion coefficients averaged for the full QENS range (B). Each box in (B) represents one standard deviation with the internal line denoting the mean, open symbols represent the mode, the 'x' symbols denote the extremes.

non-functionalized and VA-functionalized Nafion. Much larger self-diffusivities measured by QENS than by PFG NMR were also previously observed for water diffusion in Nafion.[42–44] Clearly, such data indicate the existence of areas of fast local mobility on the nanometer length scale probed by QENS. These areas are separated by transport barriers leading to the much lower self-diffusivities on the micrometer length scale measured by PFG NMR. It is important to note, however, that the self-diffusivities measured by both techniques for displacements smaller than the micrometer-sized domains were not appreciably changed by the VA-functionalization. This result can be explained by the expectation that only a small fraction of acetone molecules in Nafion is expected to interact with VA at any particular time.

4. Conclusions

In summary, we report the PFG NMR and QENS diffusion data showing that the VA functionalization does not lead to any significant changes in the water and/or acetone self-diffusivities when they are measured for the same or similar displacements smaller than the dimensions of micrometer-sized domains of interconnected water channels. These techniques probe very different length scales of displacements (nm by QENS and μm by PFG NMR). Hence, the much large acetone self-diffusivities measured by QENS than by PFG NMR under the same or similar conditions are explained by a difference in the Nafion transport properties on different length scales. The reported PFG NMR data present evidence that the VA functionalization leads to a better separation of the diffusion pathways of water and acetone. While water molecules mostly diffuse along water channels and acetone molecules mostly diffuse in the interfacial regions even in VA free Nafion,[19] the functionalization with this acid leads to a stronger preference of water and acetone to their respective regions during the diffusion process. As a result, the diffusion processes of water and acetone can become more independent from each other in VA-functionalized Nafion membranes. This conclusion is based on the reported PFG NMR data showing a different influence of acetone concentration in the membranes with and without VA on the water permeance of the interfaces between neighboring domains of interconnected water channels. This finding from the diffusion studies is correlated with the SAXS structural characterization measurements indicating that the addition of the acid functionalization causes swelling of interfacial PFE regions and, at the same time, water channel compression. Such influence was previously attributed to guest molecules being located in the PFE side chain regions of the Nafion polymer, between the crystalline backbone and the hydrophilic water channels.[19] Hence, it is reasonable to conclude that VA molecules in the studied membranes are also located in these regions. Larger for acetone than for water decrease in the NMR relaxation times upon the VA addition is consistent with this conclusion. This may explain the role of VA in preserving catalytic activity in the presence of water.[10] The ability to control and separate better the diffusion pathways of different types of molecules in Nafion by introducing immobilized species is expected to be of growing importance in novel applications of Nafion such as chemical sensing. Such control is facilitated by understanding the relationship between microscopic structural and transport properties of Nafion membranes, and can accelerate development of new applications involving molecular intramembrane transport.

Conflicts of interest

There are no conflicts to declare.

Acknowledgements

This research has been made possible by NSF awards CBET-1836551 and CBET-1836556. A portion of this work was performed in the McKnight Brain Institute at the National High Magnetic Field Laboratory's Advanced Magnetic Resonance Imaging and Spectroscopy (AMRIS) Facility, which is supported by National Science Foundation Cooperative Agreement no.

DMR-1644779 and the State of Florida. This work was supported in part by an NIH award, S10RR031637, for magnetic resonance instrumentation. The following instrument scientists are acknowledged: Eugene Mamontov, Christopher Stanley, Soenke Seifert. A portion of this research used resources at the Spallation Neutron Source, as appropriate, a DOE Office of Science User Facility operated by the Oak Ridge National Laboratory. This research used resources of the Advanced Photon Source, a U.S. Department of Energy (DOE) Office of Science User Facility operated for the DOE Office of Science by Argonne National Laboratory under Contract No. DE-AC02-06CH11357.

References

1 K. D. Kreuer, *J. Membr. Sci.*, 2001, **185**, 29–39.
2 S. J. Peighambardoust, S. Rowshanzamir and M. Amjadi, *Int. J. Hydrogen Energy*, 2010, **35**, 9349–9384.
3 M. Skyllas-Kazacos, M. H. Chakrabarti, S. A. Hajimolana, F. S. Mjalli and M. Saleem, *J. Electrochem. Soc.*, 2011, **158**, R55.
4 H. Zhang and P. K. Shen, *Chem. Rev.*, 2012, **112**, 2780–2832.
5 T. Sata, T. Sata and W. Yang, *J. Membr. Sci.*, 2002, **206**, 31–60.
6 T. Luo, S. Abdu and M. Wessling, *J. Membr. Sci.*, 2018, **555**, 429–454.
7 F. Tailoka, *Solid State Ionics*, 2003, **161**, 267–277.
8 P. D. van der Wal, N. F. de Rooij and M. Koudelka-Hep, *Sens. Actuators, B*, 1996, **35**, 119–123.
9 A. D. Worrall, J. A. Bernstein and A. P. Angelopoulos, *Talanta*, 2013, **112**, 26–30.
10 A. D. Worrall, Z. Qian, J. A. Bernstein and A. P. Angelopoulos, *Anal. Chem.*, 2018, **90**, 1819–1826.
11 K. Schmidt-Rohr and Q. Chen, *Nat. Mater.*, 2008, **7**, 75–83.
12 T. D. Gierke, G. E. Munn and F. C. Wilson, *J. Polym. Sci.*, 1981, **19**, 1687–1704.
13 K. A. Mauritz, *J. Macromol. Sci.*, 1988, **28**, 65–98.
14 J. T. Wescott, Y. Qi, L. Subramanian and T. W. Capehart, *J. Chem. Phys.*, 2006, **124**, 134702.
15 A. B. Yaroslatev, *Polym. Sci., Ser. A*, 2013, **55**, 674–698.
16 A. Kusoglu and A. Z. Weber, *Chem. Rev.*, 2017, **117**, 987–1104.
17 R. Hiesgen, I. Wehl, E. Aleksandrova, E. Roduner, A. Bauder and K. A. Friedrich, *Int. J. Energy Res.*, 2009, **34**, 1223–1238.
18 J. T. Hinatsu, *J. Electrochem. Soc.*, 1994, **141**, 1493.
19 S. J. Berens, A. Yahya, J. Fang, A. Angelopolous, J. D. Nickels and S. Vasenkov, *J. Phys. Chem. B*, 2020, **124**, 8943–8950.
20 D. Lopez, J. Goodwinjr and D. Bruce, *J. Catal.*, 2007, **245**, 381–391.
21 B. Corain, M. Zecca and K. Jeřábek, *J. Mol. Catal. A: Chem.*, 2001, **177**, 3–20.
22 A. Krueger, W. Balcerowiak and E. Grzywa, *React. Funct. Polym.*, 2000, **45**, 11–18.
23 U.-O. Badmaarag, J. A. Bernstein, R. Shekarriz and A. P. Angelopoulos, *Sens. Bio-Sens. Res.*, 2020, **29**, 100373.
24 Y. Q. Zhang, F. Guo, Q. Cui, M. Y. Lu, X. L. Song, H. J. Tang and Q. S. Li, *J. Chem. Eng. Data*, 2016, **61**, 420–429.
25 R. Hammer, M. Schonhoff and R. M. Hansen, *J. Phys. Chem. B*, 2019, **123**, 8313–8324.
26 R. M. Cotts, M. J. R. Hoch, T. Sun and J. T. Markert, *J. Magn. Reson.*, 1989, **83**, 252–266.
27 S. J. Gibbs and C. S. Johnson Jr., *J. Magn. Reson.*, 1991, **93**, 395–402.
28 J. Kärger, D. M. Ruthven and D. N. Theodorou, *Diffusion in Nanoporous Materials*, Wiley-VCH, Weinheim, 2012.
29 E. Mamontov and K. W. Herwig, *Rev. Sci. Instrum.*, 2011, **82**, 085109.
30 O. Arnold, J.-C. Bilheux, J. M. Borreguero, A. Buts, S. I. Campbell, L. Chapon, M. Doucet, N. Draper, R. F. Leal and M. A. Gigg, *Nucl. Instrum. Methods Phys. Res., Sect. A*, 2014, **764**, 156–166.
31 R. T. Azuah, L. R. Kneller, Y. Qiu, P. L. W. Tregenna-Piggott, C. M. Brown, J. R. D. Copley and R. M. Dimeo, *J. Res. Natl. Inst. Stand. Technol.*, 2009, **114**, 341.
32 X. Ren, T. E. Springer and S. Gottesfeld, *J. Electrochem. Soc.*, 2000, **147**, 92.
33 A. Balwani and E. M. Davis, *ACS Appl. Polym. Mater.*, 2019, **2**, 40–54.
34 V. Baglio, A. S. Aricò, V. Antonucci, I. Nicotera, C. Oliviero, L. Coppola and P. L. Antonucci, *J. Power Sources*, 2006, **163**, 52–55.
35 R. Mueller, V. Hariharan, C. Zhang, R. Lively and S. Vasenkov, *J. Membr. Sci.*, 2016, **499**, 12–19.
36 S. Vasenkov and J. Kärger, *Microporous Mesoporous Mater.*, 2002, **55**, 139–145.
37 J. E. Tanner, *J. Chem. Phys.*, 1978, **69**, 1748–1754.
38 J. Kärger, M. Avramovska, D. Freude, J. Haase, S. Hwang and R. Valiullin, *Adsorption*, 2021, **27**, 453–484.
39 A. Kusoglu, M. A. Modestino, A. Hexemer, R. A. Segalman and A. Z. Weber, *ACS Macro Lett.*, 2012, **1**, 33–36.
40 G. Gebel, S. Lyonnard, H. Mendil-Jakani and A. Morin, *J. Phys.: Condens. Matter*, 2011, **23**, 234107.
41 H. Mendil-Jakani, S. Pouget, G. Gebel and P. N. Pintauro, *Polymer*, 2015, **63**, 99–107.
42 A. M. Pivovar and B. S. Pivovar, *J. Phys. Chem. B*, 2005, **109**, 785–793.
43 J.-C. Perrin, S. Lyonnard and F. Volino, *J. Phys. Chem. C*, 2007, **111**, 3393–3404.
44 N. Martinez, A. Morin, Q. Berrod, B. Frick, J. Ollivier, L. Porcar, G. Gebel and S. Lyonnard, *J. Phys. Chem. C*, 2018, **122**, 1103–1108.
45 V. F. Sears, *Neutron News*, 1992, **3**, 26–37.

